NJC

Accepted Manuscript

This article can be cited before page numbers have been issued, to do this please use: S. V. Bondarchuk, M. Carrera, M. de la Viuda and A. Guijarro, *New J. Chem.*, 2018, DOI: 10.1039/C7NJ04726F.

ROYAL SOCIETY OF CHEMISTRY

rsc.li/njc

View Article Online
DOI: 10.1039/C7NJ04726F

NJC

ARTICLE

Spontaneous disproportionation of lithium biphenyl in solution. A combined experimental and theoretical study†

Received 00th January 20xx,
Accepted 00th January 20xx

DOI: 10.1039/x0xx00000x

www.rsc.org/

Sergey V. Bondarchuk,[b] Manuel Carrera,[a] Mónica de la Viuda,[a] and Albert Guijarro*[a]

In the present paper we report experimental and theoretical evidence for lithium biphenyl disproportionation in solution. The presence of an absorption band (at 250 nm), which corresponds to neutral biphenyl in the spectra of dissolved crystalline $[Li^+(THP)_4][Bph^{\bullet-}]$ (1) clearly suggests the disproportionation of the biphenyl radical anion into neutral biphenyl plus the corresponding dianion, $2Bph^{\bullet-} \rightleftarrows Bph^{2-} + Bph^0$. The experimental spectrum of **1** displays four main groups of bands at 834, 644, 408 and 250 nm. Upon addition of an excess of lithium, the biphenyl band becomes diminished revealing a hidden lower intensity band at 262 nm, this one truly belonging to the dianion. Highly accurate time-dependent density functional theory (TDDFT) calculations of the electronic spectra of a series of contact as well as solvent separated ionic associate models, performed at the wB97XD/6-311++G(3df, 3pd) level of theory in dimethoxyethane (DME) solution, revealed that the contact lithium biphenyl dianion $[(Li^+DME)_2Bph^{2-}]$ predicts all the main absorption bands fairly well, while the corresponding radical anion does not reproduce the experimental spectral pattern. Analysis of the electron density distribution performed by means of Quantum Theory of Atoms in Molecules (QTAIM) confirm that the studied ionic associates represent the correct resonance structures since the charges of the lithium cations are close +1 in all the cases. Solvation usually plays a key role in these type of equilibria, however the underlying cause of this disproportionation seems to lie on the inherent electronic stabilities of the anionic species involved, as could be inferred from reported free energy calculations of the nude ion associates, neglecting any solvent effects.

Introduction

In spite of being reported almost a century ago,[1] the adducts of biphenyl and alkali metals in solution are still the subject of many studies concerning their underlying nature, with lithium occupying a central role due to its technological applications.[2] For instance, biphenyl is used as additive in commercial lithium-ion battery formulations as an overcharge protection agent, intended to prevent smoke, flames or explosions upon overvoltage regimes, enhancing their security.[3] But more specifically, lithium biphenyl adducts in solution are the active element of a promising concept in energy storage called lithium liquid anode batteries.[4] The liquid anode consist of a solution of lithium biphenyl in tetrahydrofuran (THF) as organic solvent containing additional lithium salts to improve the conductivity, and provided with an inert collecting electrode immersed. The system performs as an anodic lithium reservoir that, in addition of rechargeable, being a liquid the anode is also refuelable. These interesting applications make it worthwhile to pursue a better understanding of these adducts from every possible viewpoint. A historical perspective offer us some early representations of the lithium biphenyl adducts that are remarkably intuitive (Fig. 1a), showing a quinoid structure of a dianion with covalent lithium bonds in compliance with the valence bond theory at the time. The advent of electron spin resonance and resulting characterization of stable arene radical anions introduced them as key elements in the description of these solutions. Biphenyl radical anion was characterized as a stable open-shell species with an extra electron integrated in the π-electron system and distributed all over the molecule,[5,6,7] forming different types of ionic pairs with alkali ions, e.g. with lithium.[8] This is since then the most prevalent picture of the dominant species present in these solutions (Fig. 1b-c),[9] with few exceptions (Fig. 1d),[10] which are on the other hand devoid of an adequate characterization of a potential dianionic species.

In the course of our former synthetic studies, we noticed some reactivity aspects of the lithium biphenyl solutions prepared with an excess of lithium that were better interpreted in terms of the biphenyl dianion chemistry rather than the biphenyl radical anion. These involved nucleophilic substitution,[11] and carbolithiation of alkenes.[12] It became apparent that these intense blue-green solutions displayed an intricate behavior highly dependent on the experimental con-

[a] Departamento de Química Orgánica and Instituto Universitario de Síntesis Orgánica, Unidad asociada del CSIC, Universidad de Alicante, San Vicente del Raspeig, 03690, Alicante, Spain
[b] Department of Chemistry and Nanomaterials Science, Bogdan Khmelnitsky Cherkasy National University, blvd. Shevchenko 81, 18031 Cherkasy, Ukraine

† Electronic Supplementary Information (ESI) available: the complete list of QTAIM parameters and Fukui functions, molecular orbitals and additional calculated and experimental spectral data. See DOI: 10.1039/x0xx00000x

View Article Online
DOI: 10.1039/C7NJ04726F

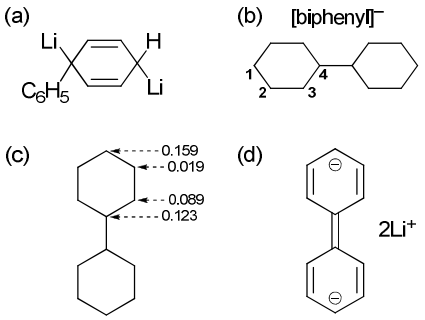

Fig. 1 Early representation of lithium biphenyl adducts: a) by Schlenk and Bergmann (1928).[1] Naked radical anion; b) by Hoijtink (1957),[6] and c) by De Boer and Weissman (1958),[7] indicating only 4 non-equivalent carbon atoms and showing the squared Hückel LUMO coefficients of biphenyl; d) Explicit dianion represented by Eisch (1963).[10]

ditions that could not be fully attributed to a single species but rather to an equilibrium of several ionic species including mono and dianions, more or less associated in the form of different ion pairs.[13] Biphenyl has indeed the most negative second reduction potential measured (i.e. giving rise to the dianion) among polycyclic arenes,[14] to the point that it rivals with the alkali metals including lithium itself.[15] This remarkable property allows the occurrence of incompletely shifted heterogeneous equilibria of formation/dissociation of the reduction adducts even in the presence of an excess of metal, the composition and dynamics of which strongly depend on the metal, the solvent and the temperature, the case of sodium being particularly well studied.[16] In the present study, we undertook the task of studying the lithium biphenyl solution in 1,2-dimethoxyethane (DME) from its UV-vis absorption spectrum, both experimentally as well theoretically, analyzing thoughtfully the results by means of TDDFT to try to identify the different lithium biphenyl adducts by their electronic transitions. Lithium and DME is a particularly well suited system for our purposes, maximizing the reducing strength of the mixture and shifting the equilibria of Scheme 1 to the right.

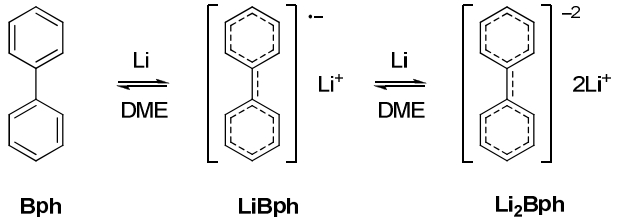

Scheme 1 Equilibria of formation of lithium biphenyl adducts in DME solution.

Results and Discussion

UV-vis spectra of lithium biphenyl DME solutions of increasing lithium content

The first UV-vis absorption spectra of lithium biphenyl were reported by Hoijtink et al.[17] The spectra recorded in THF were attributed to a free mononegative biphenyl ion ($Bph^{\bullet-}$) with lithium as countercation.[18] In general, variations in the degree of ion pairing have been proposed to justify small differences in the appearance of the spectra with other cations like sodium, while potassium displays very similar spectrum to that of lithium biphenyl in THF.[19] Hoijtink's spectrum has been widely regarded as an archetypal reference for biphenyl radical anion.[20] In Fig. 2, the experimental UV-vis spectra of mixtures of lithium and biphenyl in DME at 25 ºC covering different formal stoichiometries are shown. A spectroscopic set up with a 0.01 mm path allowed us to record over the whole 210-1100 nm wavelength range, including the regions near the solvent cut off (*ca*. 215 nm). The characteristic, well known main absorptions of a lithium biphenyl adduct at λ_{max} = 644 and 408 nm are patent. These two main peaks are dominant in all the spectra recorded. An additional shoulder at λ_{max} = 834 nm (wavelength obtained by spectral deconvolution) as well as some other small transitions are also noticeable and will be analyzed later on. A careful inspection at shorter wavelengths reveals some important insights. Often overlooked, the biphenyl absorption at λ_{max} = 250 nm is clearly visible as expected for the 0.5:1 Li:biphenyl ratio (in green) but importantly also for the 1:1 ratio (in light blue) which formally would correspond to the spectrum of the radical anion. Interestingly, this absorption at 250 nm is depleted at the 2:1 Li:biphenyl ratio (in dark blue), becoming replaced by another peak with λ_{max} = 262 nm, which persists upon reaction with a large excess of lithium (purple spectrum). Provided that reaction times are not over extended to prevent decay of the adduct by reaction with the solvent (*ca*. within 30 min under our experimental conditions),[21] and temperature does not raise (above 40-50º lithium metal segregates visibly out of the adduct solution),[22] all the spectra of lithium biphenyl adducts with stoichiometry 2:1 or above look much the same, excluding the possibility of adducts with higher Li/biphenyl ratios.

UV-vis spectra of the DME solutions of crystalline lithium biphenyl radical anion

Collected experimental evidence points towards a spontaneous disproportionation equilibrium of the lithium biphenyl radical anion species significantly shifted to the right by DME (Scheme 2). An important piece of evidence on the position of the disproportionation equilibrium of Scheme 2 may come from the analysis of isolated crystalline lithium biphenyl radical anion when taken into solution. A crystal structure of a lithium biphenyl radical anion complex, in particular the solvent-separated ion pair $[Li^{+}(THP)_4][Bph^{\bullet-}]$ (**1** in Fig. 3, THP stands for tetrahydropyran) which crystallizes out of these blue solutions has been recently reported.[13]

View Article Online
DOI: 10.1039/C7NJ04726F

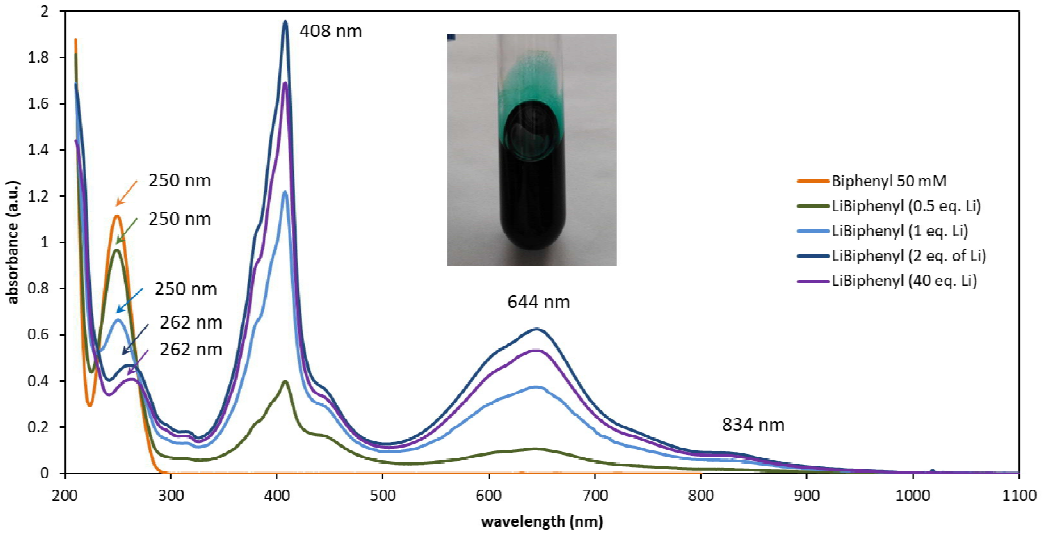

Fig. 2 Experimental UV-vis spectra of lithium biphenyl mixtures in DME (50 mM) at 25 °C using different Li/biphenyl ratios, and characteristic colour of these solutions (insert). It is noticeable that the main features of the visible absorption peaks at 644 and 408 nm remain unchanged, even for substoichiometric amounts of lithium. Near the solvent cut-off, the 250 nm absorption corresponding to the hydrocarbon biphenyl is clearly visible at the 1:1 ratio (or below), while it becomes replaced by a new, less intense absorption at 262 nm when the ratio of Li/biphenyl is 2:1 (or above). The spectrum with 40 eq. of Li (in purple) has been slightly compressed (15%) to avoid overlap with that of 2.0 eq. of Li (dark blue); they are identical within experimental error.

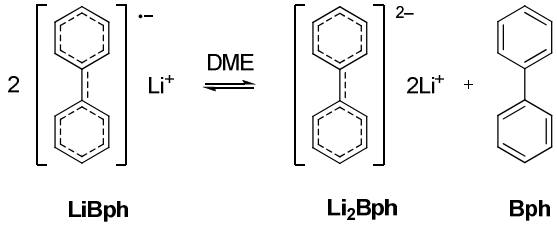

Scheme 2 Disproportionation equilibrium of lithium biphenyl in solution.

A second crystal structure of another ion pair [$Li^+(\kappa^3$-18-crown-6)$(THF)_2$][$Bph^{\bullet-}$] including both THF and tridentate 18-crown-6 in the lithium coordination sphere is also available.[19] The internal coordinates of the anionic [$Bph^{\bullet-}$] moiety are very similar in both crystals, with deviations in the biphenyl geometry of less than 1%. A scoop of crystalline **1** was dissolved in DME at 25 °C and a spectrum of the solution was recorded (Fig. 3, bottom spectrum in dark blue). For comparison, the spectrum of a 1:1 mixture of lithium and biphenyl under the same conditions is included (Fig. 3, top spectrum in light blue). Both preparations afford essentially the same spectra, with the same relative intensity between main peaks. Again the absorption of λ_{max} = 250 nm corresponding to the hydrocarbon biphenyl is clearly visible, in spite that no free biphenyl is present in the sample when starting from **1**.

Disproportionation equilibria of organic radical anions is a known issue that may be very dependent on the solvent and conditions and not easy to interpret, as evidenced by other studies with related compounds. For instance, lithium tetracene disproportionation constant expands over ten

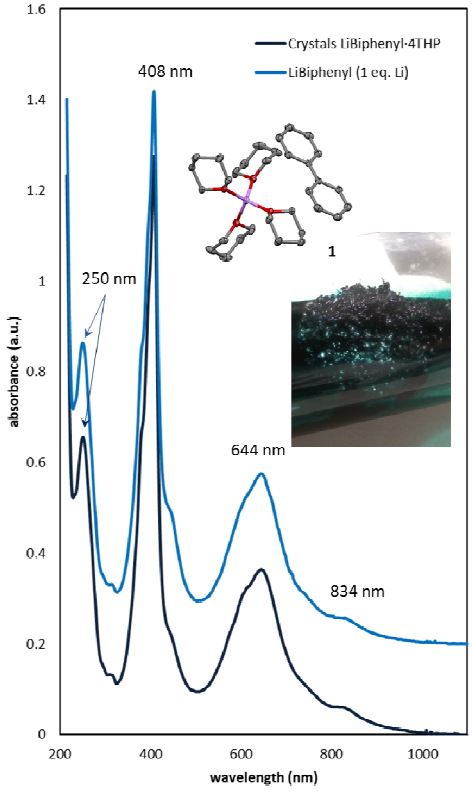

Fig. 3 Experimental UV-vis spectra of a saturated solution of crystals of [$Li^+(THP)_4$][$Bph^{\bullet-}$] (**1**) (in dark blue), and Li/biphenyl 1:1 ratio (shifted up 0.2 a. u., in light blue) in DME at 25 °C. Both spectra are nearly identical. The 250 nm absorption corresponding to the hydrocarbon biphenyl is clearly visible.

View Article Online
DOI: 10.1039/C7NJ04726F

orders of magnitude in going from tetrahydrofuran to diethyl ether.[23] In the case of lithium biphenyl considered in here, the disproportionation driving force seems to arise from the intrinsic electronic stability of the species involved in the equilibrium (Scheme 2). Using reported thermodynamic data in vacuum at the B3LYP/6-311++G(d, p) level,[13, 32] the calculated free energy of disproportionation of the equilibrium 2LiBph ⇄ Li_2Bph + Bph turns out to be definitively exergonic, roughly ΔG°_{disp} = −34 kJ mol^{-1}. This suggests an inherent electronic destabilization of the radical anion in favor of its closed shell disproportionation products, the dianion and neutral hydrocarbon, which occurs even in the absence of any solvent effects.

Structure and QTAIM analysis of the model ionic associates

We moved next to the theoretical study of Li_2Bph and LiBph in DME in order to search for the electronic transitions that best match the reported spectrum. We used DME as a solvent due to its high solvating energy with the lithium cation,[16] maximizing hence the shift of the reaction towards highly reduced products while maintaining at a reasonable level the complexity of the calculations of the different adducts. On the other hand, DME has a structural motif akin to crown ethers which were successfully employed for lithium coordination.[19] Thus, it is obvious that in the case of ionic associates like $(Li^+)_2Bph^{2-}$ and $Li^+Bph^{\bullet-}$ the effect of positive charge quenching by means of the DME molecules should take place likewise. Therefore, for the appropriate UV-vis spectra prediction we have built the model ionic associates of these ionic pairs which include one explicit DME molecule per the lithium cation, i.e. contact ion pairs [$(Li^+DME)_2Bph^{2-}$] and [$(Li^+DME)Bph^{\bullet-}$] (Fig. 4), as well as two explicit DME molecules per lithium cation, i.e. solvent separated ion pairs [$Li^+(DME)_2]_2[Bph^{2-}$] and [$Li^+(DME)_2][Bph^{\bullet-}$] (Fig. 5). The equilibria of such contact ion pairs have been previously discussed.[13]

When calculating systems which consist of several separated fragments in terms of single reference approach, like DFT(B3LYP), one should keep in mind the known problem of the appropriate resonance structure description.[24,25] To distinguish resonance structures, one can analyze atomic charges and bond lengths in the biphenyl fragment since these are strongly related to the oxidized state of the latter.[24] The calculated bond lengths in any of the LiBph ion pair is very close to ones obtained by X-ray analysis of the solid complexes with the crown ethers.[19] The calculated *vs* experimental (in parentheses) bond lengths in the biphenyl fragment of the contact ion pair [$(Li^+DME)Bph^{\bullet-}$] are the following: C9–C9' 1.442 (1.433) Å, C9–C10 1.448 (1.438) Å, C10–C11 1.383 (1.377) Å and C11–C12 1.420 (1.393) Å. The obtained QTAIM charges (q_A, in a.u.) at the lithium and selected carbon atoms are presented in Fig. 6. The q_A values also indicate that the calculated ionic pairs [$(Li^+DME)_2Bph^{2-}$] and [$(Li^+DME)Bph^{\bullet-}$] are described well. The charges at the lithium cations are close to +1 (Fig. 6); therefore the partition of the electron density is made properly.

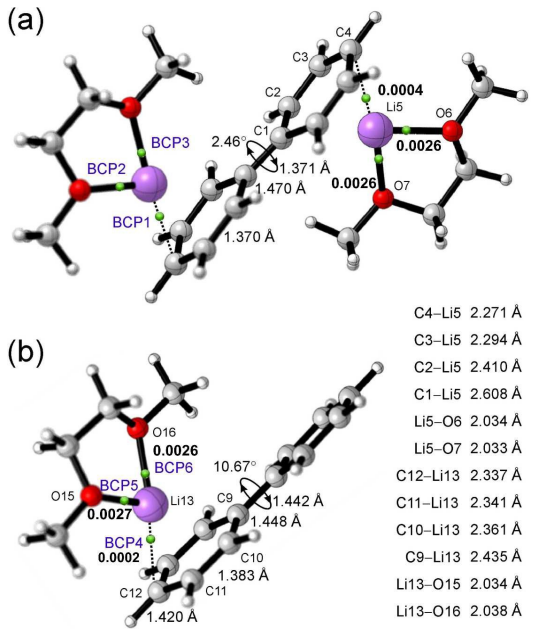

Fig. 4 The optimized contact ionic associates of the lithium cation with the biphenyl dianion [$(Li^+DME)_2$ Bph^{2-}] (a) and radical anion [$(Li^+DME)Bph^{\bullet-}$] (b).

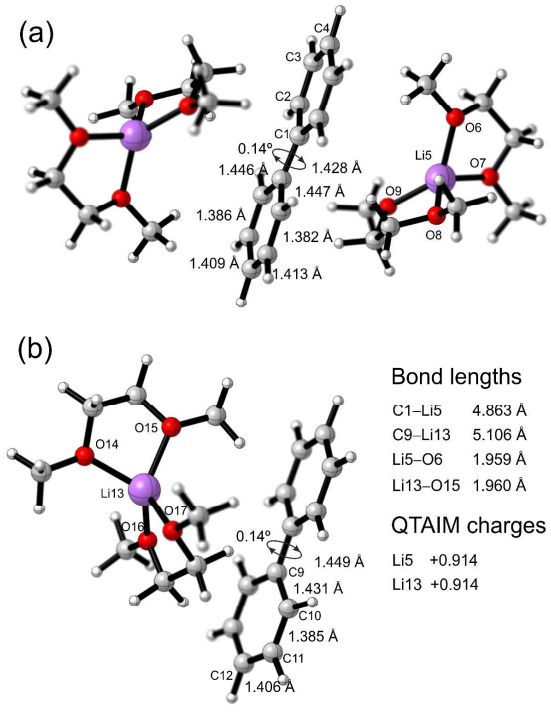

Fig. 5 The optimized solvent separated ionic associates of the lithium cation with the biphenyl dianion [$Li^+(DME)_2]_2[Bph^{2-}$] (a) and radical anion [$Li^+(DME)_2][Bph^{\bullet-}$] (b).

View Article Online
DOI: 10.1039/C7NJ04726F

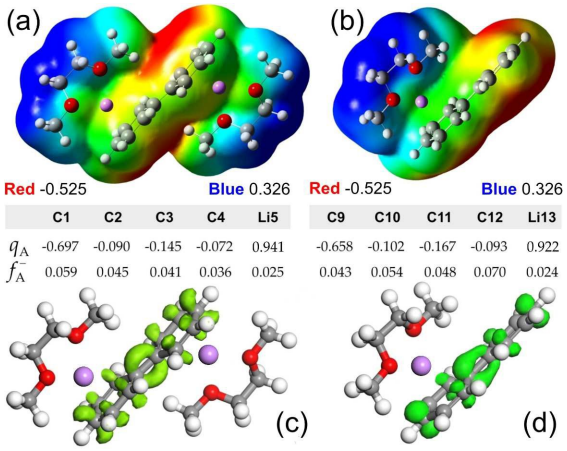

Fig. 6 Molecular electrostatic potential (MEP) isosurfaces (a, b) and main contributions of the nucleophilic Fukui function f^+ (c, d). Tabulated values include QTAIM charges (q_A, in a.u.) and the condensed Fukui functions (f_A^+).

For the solvent separated ion pair $[Li^+(DME)_2][Bph^{\bullet-}]$, the calculated *vs* experimental bond lengths are: C9–C9' 1.449 (1.433) Å, C9–C10 1.431 (1.438) Å, C10–C11 1.385 (1.377) Å and C11–C12 1.406 (1.393) Å, which shows a very similar, only slightly better correspondence to the experimental. Thus, we can conclude that the calculated structural results are valid. Again, the QTAIM charges at the lithium cations equal +0.914 in both solvent separated ion pairs (Fig. 5), which means that the wave function reflects the correct description of electron density. On the other hand, the use of such solvent separated ion pairs for the electron spectra prediction is complicated for two reasons. Firstly, the optimized structures in Fig. 5 are only a particular case for such systems. To obtain more realistic particle distribution in the $[Li^+(DME)_2]_2[Bph^{2-}]$ and $[Li^+(DME)_2][Bph^{\bullet-}]$ systems, one should apply statistical methods, like Monte Carlo or molecular dynamics with inclusion of much more solvent molecules and ions. But even in this case, other than merely Coulombic, the interaction between lithium and biphenyl will be negligible, which reflects in the complete absence of the bond critical points (BCP) between them (Fig. 5). As a result, the spectral pattern is expected to be characteristic for isolated cationic and anionic species.

Focusing now on the contact structures, π coordination to the lithium ions occurs at the typical ionic distances at about 2.5 Å (Fig. 4). The topological analysis of the electron density reveals three BCPs, between the lithium cations and the biphenyl and DME molecules (green dots in Fig. 4). To describe the nature of these bonds, we have analyzed the following QTAIM parameters, namely, electron density $\rho(r)$, its Laplacian $\nabla^2\rho(r)$ and the Hamiltonian energy density $h_e(r)$ (Table 1). The positive $\nabla^2\rho(r)$ values characterize these bonds as closed-shell interactions and the positive $h_e(r)$ quantities justify them as the ionic bonds. Energies of these bonds have been estimated using the Espinosa equation (see the Experimental Section for details). Thus, the energy of the C4–Li5 bond is 25.2 kJ and the C12–Li13 bond is 20.4 kJ. At the same time the bonding of lithium cation with the DME molecule is much stronger and equals to 62.9 kJ $[(Li^+)_2Bph^{2-}]$ and 62.2 kJ $[Li^+Bph^{\bullet-}]$. These bonds are characterized by very small Laplacian bond orders (bold values in Fig. 4). The complete presentation of the critical points and the corresponding paths are illustrated in Fig. S1 and S2 in ESI.

Table 1 The calculated QTAIM parameters (a.u.) at the BCPs in the model contact ionic associates

BCP#	$\rho(\mathbf{r})$	$\nabla^2\rho(\mathbf{r})$	$h_e(\mathbf{r})$	$g(\mathbf{r})$	$v(\mathbf{r})$
1	0.01852	0.10393	0.00340	0.02258	-0.01918
2	0.02178	0.14869	0.00668	0.03050	-0.02382
3	0.02205	0.14898	0.00659	0.03066	-0.02408
4	0.01538	0.08868	0.00333	0.01884	-0.01551
5	0.02166	0.14793	0.00667	0.03031	-0.02365
6	0.02175	0.14688	0.00651	0.03121	-0.02371

We have also built the 3D contours of the molecular electrostatic potential (MEP) of the model contact ionic associates (Fig. 6 a, b). The highest potential is located on the DME molecules and the most negative values are on the biphenyl moiety. Also we have calculated the Fukui functions for different type of attack. The obtained results specify the electrophilic attack as the most appropriate. Therefore, the nucleophilic Fukui function values condensed to the selected atoms are presented in Fig. 6. The complete list of condensed Fukui function values for different types of attack is gathered in Tables S1 and S2 and the atom labeling is presented in Fig. S3 and S4 in ESI.

Assignment of the electronic spectra of the $[(Li^+DME)_2Bph^{2-}]$ and $[(Li^+DME)Bph^{\bullet-}]$ ionic associates

The experimental absorption spectrum of the DME solution of lithium biphenyl is included in Fig. 7a. As one can see in Fig. 7a, this spectrum demonstrates several characteristic bands, which include a group of peaks at 408 nm, the red-shifted band at 644 nm and finally the shoulder at 834 nm. Preliminary TDDFT calculations revealed that the UV-vis spectrum of $[(Li^+DME)Bph^{\bullet-}]$ significantly differs in the absorption pattern (Fig. 7c). The calculated spectrum of the radical anion associate exhibits no significant absorption beyond 600 nm. The other two bands do not match with the experimentally observed bands (Fig. 7c).

In contrast, the calculated electronic spectrum of the dianion associate $[(Li^+DME)_2Bph^{2-}]$ fits rather well for all the observed bands (Fig. 7b). Thus, we have performed a series of TDDFT calculations in order to find the most appropriate functional for the UV-vis spectra prediction. The spectrum of the $[(Li^+DME)_2Bph^{2-}]$ associate demonstrates six characteristic

View Article Online
DOI: 10.1039/C7NJ04726F

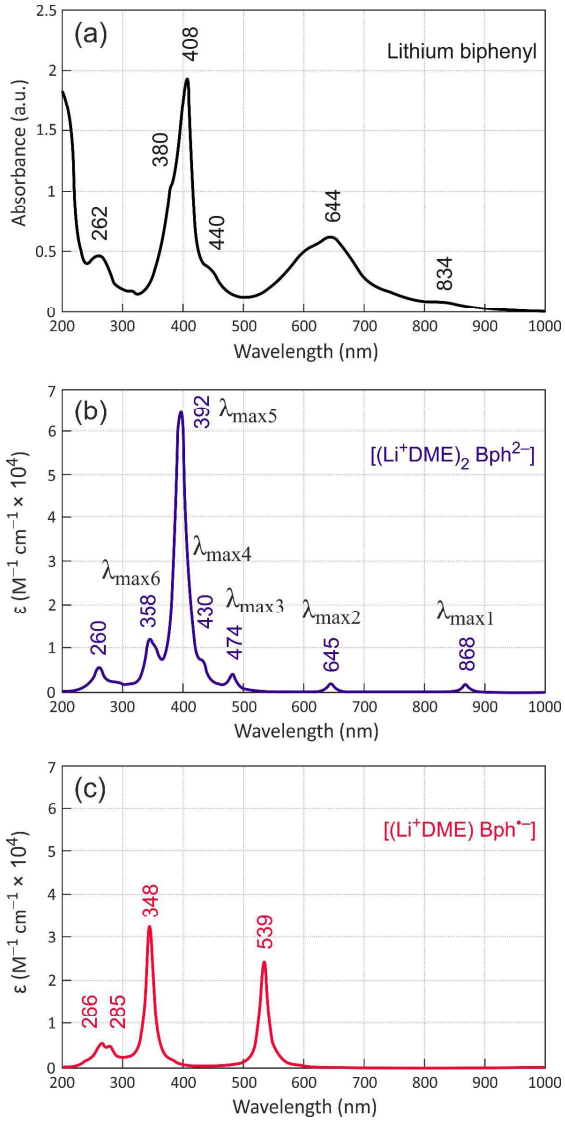

Fig. 7 Experimental absorption spectrum of the DME solution of lithium biphenyl (40:1) and the calculated UV-vis spectra of the developed model contact ionic associates at the wB97XD/6-311++G(3df, 3pd) level of theory.

peaks which are indicated in Fig. 7b as λ_{max}. The results of TDDFT calculations in DME solution at the DFT(X)/6-311++G(2d, 2p) level of theory, where X is the used functional are gathered in Table 2. As it follows from Table 2, the double hybrid functional with the dispersion correction term, namely, wB97XD produces the transition energies being the closest to the experimentally measured. Although the hybrid functional HSE06 has been recently shown to produce experimentally close band gaps and optical properties in solids,[26] it significantly underestimates the transition energies of the absorption bands, especially in the red region of the spectrum (Table 2). Conventional B3LYP as well as the pure Minnesota functional M06L behave in a similar manner.

Table 2 λ_{max} (nm) of the characteristic peaks in the UV-vis spectrum of $[(Li^+DME)_2\ Bph^{2-}]$ calculated using different functionals and the 6-311++G(2d, 2p) basis set

Functional	λ_{max1}	λ_{max2}	λ_{max3}	λ_{max4}	λ_{max5}	λ_{max6}
wB97XD	867	647	475	430	398	357
LC-wPBE	743	538	416	377	347	318
CAM-B3LYP	876	746	543	482	453	406
HSE06	1029	911	670	628	550	459
M062X	957	810	595	526	493	445
mPW1PBE	992	895	660	550	512	448
M06L	1065	1007	768	575	541	479
B3LYP	1044	1004	722	585	535	485

The complete assignments of the electronic spectra of the model ionic associates calculated at the wB97XD/6-311++G(3df, 3pd) level of theory are listed in Tables 3 and 4. We have discussed only the transitions with the oscillator strengths $f \geq 0.01$ and which have more than 10% weight. All the transitions are listed in Tables S3 and S4 and the molecular orbitals (MOs) which are involved into the electron transitions are illustrated in Fig. S5 and S6 in ESI. We should stress that isosurfaces of the MOs illustrated inside the frames are the localized MOs which enclose 0.03 a. u. of the electron density. Meanwhile, the rest MOs have strongly diffuse character and are spread throughout the ionic associate; these are built as the contours of 0.01 a. u. of the electron density. As one can see in Table 3 and Fig. S5, the S_1 transition corresponds to the π→π* local ring excitation. A similar nature has the most intense transition S_{14} at 399 nm and S_{24} at 347 nm (Fig. 7b). The rest transitions correspond to the electron excitations from the highest occupied molecular orbital (HOMO) to various diffuse MOs; thus, these transitions possess a charge transfer character. On the other hand, the UV-vis spectrum of the $[(Li^+DME)Bph^{\bullet-}]$ ionic associate demonstrates two relatively intense modes, namely, D_4 at 539 nm and D_{14} at 348 nm (Fig. 7c). These two transitions along with the D_{15} are the local ring excitations of π→π* nature. The rest transitions correspond to the charge transfer.

A relevant peak appears at 262 nm in the experimental spectrum of lithium biphenyl obtained with an excess of lithium, which does not corresponds to the neutral biphenyl molecule (Fig. 7a). To achieve this band in our theoretical study, we have calculated the energies of the first 45 singlet and doublet transitions in the electronic spectra of $[(Li^+DME)_2\ Bph^{2-}]$ and $[(Li^+DME)Bph^{\bullet-}]$, respectively (Fig. 7b, c). This band is predicted rather well for both calculated spectra. The presence of these low intensity bands at 260 nm (Fig. 7b) and 266 nm (Fig. 7c) reveals a complex form of the wave functions, which express the studied systems as charged and neutral ionic associates simultaneously.

To access additional information about the stability of the TDDFT results, we have varied the model ionic associate composition and checked the effect of the basis set expansion. For this purpose we have calculate the UV-vis spectra for the

View Article Online
DOI: 10.1039/C7NJ04726F

Table 3 Calculated UV-vis spectrum of contact lithium dianion [$(Li^+DME)_2$ Bph^{2-}] (H – the highest occupied molecular orbital, L – the lowest unoccupied molecular orbital)

State	λ, nm	*E*, eV	*f*	Assignment		
S_1	868	1.43	0.0181	H → L+8 (73%)	H → L+10 (20%)	
S_2	645	1.92	0.0198	H → L (36%)	H → L+6 (30%)	H → L+9 (15%)
S_7	475	2.61	0.0110	H → L+5 (78%)	H → L+19 (11%)	
S_8	474	2.62	0.0233	H → L+4 (53%)	H → L+20 (14%)	H → L (14%)
S_{10}	430	2.88	0.0331	H → L+9 (53%)	H → L+11 (10%)	H → L+4 (10%)
S_{12}	413	3.00	0.0138	H → L+10 (54%)	H → L+8 (16%)	
S_{13}	409	3.03	0.0550	H → L+13 (29%)	H → L+2 (17%)	H → L+11 (15%)
S_{14}	399	3.11	0.4154	H → L+11 (17%)	H → L+13 (15%)	H → L+32 (13%)
				H → L+2 (10%)	H → L+28 (10%)	
S_{16}	392	3.17	0.4168	H → L+32 (21%)	H → L+11 (12%)	H → L+6 (12%)
S_{18}	363	3.42	0.0110	H → L+18 (21%)	H → L+19 (18%)	H → L+14 (17%)
				H → L+5 (16%)		
S_{19}	358	3.47	0.0347	H → L+17 (44%)	H → L+15 (11%)	
S_{20}	354	3.51	0.0103	H → L+20 (21%)	H → L+17 (19%)	H → L+15 (16%)
				H → L+22 (11%)		
S_{23}	350	3.55	0.0277	H → L+15 (18%)	H → L+17 (13%)	H → L+21 (11%)
S_{24}	347	3.57	0.0562	H → L+15 (28%)	H → L+23 (13%)	H → L+20 (11%)
S_{42}	260	4.76	0.0439	H → L+41 (53%)	H → L+49 (14%)	

Table 4 Calculated UV-vis spectrum of contact lithium radical anion [$(Li^+DME)Bph^{\bullet -}$]

State	λ, nm	*E*, eV	*f*	Assignment		
D_4	539	2.30	0.3233	H(α) → L(α)+15 (+62%)		
D_{13}	355	3.49	0.0113	H(α) → L(α)+10 (+45%)		
D_{14}	348	3.56	0.3243	H(β) → L(β)+4 (+50%)		
D_{15}	347	3.58	0.0931	H(α) → L(α)+11 (+27%)	H(β) → L(β)+4 (18%)	
D_{16}	337	3.68	0.0123	H(α) → L(α)+12 (+15%)	H(α) → L(α)+17 (+10%)	H(α) → L(α)+14 (10%)
D_{25}	285	4.35	0.0251	H(β)–1 → L(β)+5 (+12%)	H(β)–1 → L(β)+16 (10%)	
D_{26}	280	4.44	0.0115	H(α) → L(α)+22 (+33%)	H(α) → L(α)+24 (+12%)	H(α) → L(α)+21 (+10%)
D_{31}	266	4.66	0.0360	H(β)–2 → L(β)+5 (+17%)	H(α)–3 → L(α)+4 (+10%)	
D_{33}	258	4.81	0.0136	H(β) → L(β)+16 (+28%)	H(β) → L(β)+14 (15%)	H(β)–3 → L(β)+5 (11%)

$[(Li^+)_2$ $Bph^{2-}]$ ionic associate without explicit DME molecules in both the C_{2h} and C_{2v} point groups. The optimized structures along with the topological QTAIM parameters are illustrated in Fig. S7 in ESI. It is obvious that the DME molecules possess a limited effect on the geometry of the contact ionic pair. The structure in the C_{2h} point group is more stable than the corresponding C_{2v} structure by 6.0 kJ mol^{-1}. Note that the resonance structure of the Bph^{2-} is the same as for the previously calculated biphenyl and benzidine dication.[27,28] The QTAIM properties of these contact ionic pair are listed in Table S5 in ESI. Calculations of the electronic spectra of the aforementioned associates are illustrated in Fig. S8 in ESI. As it follows from Fig. S8, the change of the Li^+ cation coordination site has a little effect on the absorption pattern. Thus, the probable errors in the model ionic associate composition can be neglected. A noticeable difference between the absorption spectra of the $[(Li^+)_2$ $Bph^{2-}]$ associate and its analogues without DME molecules is in the position of λ_{max2} (Fig. 7b and S8). In the latter case, this band is significantly red-shifted. Additionally, the numerical data on the transition energies and their assignment are listed in Tables S6 and S7 in ESI. Early attempts to interpret the spectra of a naked radical anion of biphenyl,[29] as well as a more recent approach,[30] are known. In both cases, neither the stabilizing effect of a cationic counterpart nor the solvent was included in the model.

Some remarks on vibrational spectroscopy studies of lithium biphenyl solutions

There are some attempts to describe the composition of lithium biphenyl solutions by IR vibrational spectroscopy,[31,32] a difficult task that, in addition to the high sensitivity of the samples to oxygen, humidity or simply decay by reaction with the solvent, faces the drawback of a rather limited IR spectral resolution. As noticed by Devlin et al. using codeposits of biphenyl and potassium in the solid state, there is an overlap between IR bands from different species, biphenyl and its mono and dianion, among other difficulties.[33] In spite of that,

View Article Online
DOI: 10.1039/C7NJ04726F

it is significant that the IR spectrum of the adduct with a formal composition close to the radical anion in Ref. 31 is similar to the sum of the biphenyl spectrum itself plus the adduct with a formal composition close to the dianion ($Li_{1.23}$Bph and $Li_{2.46}$Bph in Figure 3 of that reference), which is in accordance with our findings.

To the best of our knowledge, there are no reported Raman spectra of lithium biphenyl adducts, although studies with other alkali metals can be found in the literature.[20c,34] We believe that, in general, caution should be taken when interpreting Raman vibrational data from alkali metal biphenyl adducts, since the high intensity of the Raman excitatory laser radiation combined with a very high absorbance of the sample at the laser wavelength may trigger an extensive photoelectron detachment and a photostationary state dominated by the radical anion. Indeed, photoelectron detachment has been reported and described for sodium biphenyl adducts in DME.[35] For all the abovementioned reasons, we believe that the electron spectroscopy is a better suited method to study the nature of the existing adducts in these solutions, particularly when it is backed up by a consistent theoretical model explaining the observed electronic transitions.

Conclusions

We have reexamined the nature of lithium biphenyl adducts in DME (also extensible to THF, see Fig. S9) by means of UV-vis spectroscopy. Regardless of the initial Li/biphenyl ratio used in the preparation of the solutions (0.5:1, 1:1, 2:1 and 40:1), the electronic spectra always display the expected main absorptions at λ_{max} = 644 and 408 nm in the near UV and visible range of wavelengths, a likely reason for which this spectrum has been historically attributed to the biphenyl radical anion. Moving to shorter wavelengths by means of a 0.01 mm path flow cell, the absorption of biphenyl at λ_{max} = 250 nm is clearly revealed, but only in the solutions of 1:1 or lower stoichiometry, disappearing for 2:1 Li/biphenyl ratios or higher, in which case is replaced by another minor absorption at λ_{max} = 262 nm.

A spontaneous disproportionation equilibrium is consistent with the reported experimental facts. To test this without other interferences, crystalline lithium biphenyl radical anion in the form of $[Li^+(THP)_4][Bph^{\bullet-}]$ (**1**) was prepared and its UV-vis spectrum recorded in DME. The presence of a characteristic biphenyl absorption band evidences that a quickly disproportionation equilibrium has taken place upon solution. This is therefore a nice example of a dynamic system in which the main species found in solution and in the solid state are very different. To back up this hypothesis, the electronic spectra of different ionic associates involving either the radical anion or dianion of biphenyl and solvated lithium as countercation have been thoroughly analyzed by state of the art TDDFT methods and subsequent population analysis. Both contact and solvent separated ion pairs/triples were included as models. The best fit with the experimental spectrum is found for the close contact ion triple $[(Li^+DME)_2Bph^{2-}]$, which reproduces rather well the typical main spectral absorptions, as well as the new peak found in the middle UV range that shows up when neutral biphenyl is completely reacted. A complete assignment of the main electronic transitions has been carried out for the best models in each case to gain a better understanding of the experimental electronic spectrum. From the similarities in the reported UV-vis spectra of sodium biphenyl and potassium biphenyl,[17,19] it is safe to say that disproportionation and overreduction to the dianion is occurring in these cases too, although each one to a different extent; sodium has the less negative reduction potential among the alkali metals, hence providing the lowest dianion concentrations in the final mixtures, while potassium is closer to lithium in that aspect.

Experimental Section

Preparation of samples for UV-vis spectroscopy

All air and moisture sensitive reactions and manipulations were carried out under dry argon atmosphere using standard Schlenk lines and a glovebox when necessary. DME, THF and THP were dried and distilled over Na/K alloy right before use. Best grade commercially available biphenyl (99.5%, Sigma-Aldrich) was used without further purification. Lithium powder was prepared from lithium granules (99%, Sigma-Aldrich) using an impact grinding mill, cleansed by stirring with a diluted solution of biphenyl in DME, taken up and rinsed with dry DME before using. All glassware was dried in an oven at 100 °C and cooled to room temperature under argon before use. A double beam UV-vis spectrophotometer (Shimadzu UV-1603) was used for spectra recording.

Dark greenish-blue solutions of LiBiphenyl in DME of Fig. 2 were prepared by reaction of a carefully weighted mixture of lithium and biphenyl with the corresponding Li/biphenyl ratios and freshly distilled solvent enough to make a 50 mM solution using magnetic stirring at 25 °C, which was continued until the reaction with lithium went to completion (less than *ca*. 30 min). When a large excess of lithium was used (40 eq), the reaction tube was centrifuged (2500 rpm, 2 min) to float the excess of lithium. Centrifugation proved to be very efficient separating unwanted dispersed particles; a perfectly clear, deeply coloured solution was used in all cases. A Starna short path flow cell (Spectrosil®quartz, 0.01 mm path length) provided with a brass three-way stopcock valve was connected both to the reaction tube and to a dry argon cylinder. The system was fluxed with argon and the adduct solutions were smoothly pumped through the cell located inside the spectrophotometer, wherein an analogous open-ended cell was mounted in parallel for solvent blank subtraction.

Crystals of $[Li^+(THP)_4][Bph^{\bullet-}]$ (**1**) were prepared as stated elsewere,[13] rinsed with dry hexane, drained and transferred inside a glovebox to prepare the corresponding solutions that were analyze in the same way as explained above.

Quantum-chemical calculations

View Article Online
DOI: 10.1039/C7NJ04726F

Density functional theory (DFT)[36] calculations presented in this paper are performed using GAUSSIAN09 suite of programs.[37] For geometry optimizations and the corresponding vibrational spectra calculations we have applied the hybrid exchange-correlation functional B3LYP[38,39] with the Pople's split-valence quasi triple-ζ, in the valence shell basis set (6-311 G) and addition of both polarization (2d,2p) and diffuse (++) functions.[40] All the calculated structures have been justified as minima on a potential energy hypersurface. Simulation of the condensed (liquid phase) conditions have been performed by means of the polarizable continuum model (PCM) in the conductor-like formalism (CPCM).[41] To define cavities the universal force field (UFF) radii have been used. The custom defined PCM parameters, ε = 7.2 D and ε_{inf} = 1.903296, have been specified to define an additional solvent dimethoxyethane (DME).

For the UV-vis spectra calculations the time-dependent density functional theory (TDDFT) has been used entirely.[42] For this purpose we have used a more expanded basis set, namely, 6-311++G(3df,3pd). To find the most appropriate functional for the spectra prediction, we have applied a set of trials. Among the tested methods we have selected pure, hybrid and range-separated functionals with and without dispersion correction terms and including different amounts of the Hartree-Fock exchange. The used functionals are the following: B3LYP, wB97XD,[43] LC-wPBE,[44] CAM-B3LYP,[45] HSE06,[46] M062X,[47] mPW1PBE[48] and M06L.[49] Fitting the electronic absorption spectra curves were performed using the Gauss distribution function and a half-width of 3000 cm^{-1} with the SWizard 5.0 program package.[50]

The calculations of Quantum Theory of Atoms in Molecules (QTAIM)[51] properties have been carried out by means of the AIMQB program within the AIMStudio program suite using the Proaim basin integration method.[52] Post-SCF analyses have been performed using recently developed Multiwfn 3.3.7 program package.[53] Bond orders were determined using the recently developed scheme which undergoes the Laplacian of the electron density values $\nabla^2\rho(\mathbf{r})$ (eq. 3).[54]

$$L_{A,B} = -10 \times \int_{\nabla^2\rho<0} w_A(\mathbf{r}) w_B(\mathbf{r}) \nabla^2\rho(\mathbf{r}) \mathrm{d}\mathbf{r} \quad (3)$$

where *w* is a smoothly varying weighting function proposed by Becke and represents fuzzy atomic space.[54]

Energies of the weak intermolecular interactions including the energies of ionic associates have been estimated using electron density values *v*(**r**) by means of the Espinosa equation (eq. 4)

$$E = 1312.75 v(r) \text{, kJ mol}^{-1}, \quad (4)$$

Herein, *v*(**r**) is the potential energy density at the corresponding bond critical point.[55]

Condensed Fukui functions have been calculated using the atomic charges determined by the Hirshfeld population analysis.[56] These calculations have been carried out using the PBE[57] functional and the numerical basis set TNP[58] with the DMol^3 program[59] implemented in Materials Studio 7.0 suite of programs.[60] The polar medium simulation have been performed using a conductor-like screening model (COSMO).[61]

Conflicts of interest

There are no conflicts to declare.

Acknowledgements

Financial support by the Spanish Ministry of Economy and Competitiveness (Grant No. MAT2016-78625-C2-2-P), the Ministry of Education and Science of Ukraine, Research Fund (Grant No. 0113U001694), the Generalitat Valenciana (Grant PROMETEO/2017/139) and the University of Alicante is gratefully acknowledged. MC thanks the VIDI of the University of Alicante for a predoctoral grant. AG greatly appreciates the computational resources provided by the Department of Applied Physics of the University of Alicante.

Notes and references

1 W. Schlenk and E. Bergmann, *Ann. Chem.* 1928, **463**, 1-97.
2 M. Ue, *Role Assigned Electrolytes: Additives*, in *Lithium-Ion Batteries,* M. Yoshio, R. J. Brodd, A. Kozawa Eds., Springer Science+Business Media, LLC 2009, p. 96-101.
3 S. S. Zhang, *J. Power Sources.*, 2006, **162**, 1379-1394.
4 a) A. Rinaldi, Y. Wang, K.S. Tan, O. Wijaya and R. Yazami, *Lithium-air batteries for medium- and large-scale energy storage*, in *Advances in Batteries for Medium- and Large-Scale Energy Storage, 1st Ed.*, C. Menictas, M. Skyllas-Kazacos, T. M. Lim, Eds., Elsevier Ltd. 2015, p. 387, 395-396. b) R. Yazami, *Hybrid Electrochemical Generator With A Soluble Anode*, US Patent 20100141211A1.
5 E. de Boer, *J. Chem. Phys.* 1956, **25**, 190-190.
6 G. J. Hoijtink, *Mol. Phys.* 1958, **1**, 157-162.
7 E. de Boer and S. I. Weissman, *J. Am. Chem. Soc.* 1958, **80**, 4549-4555.
8 H. Nishiguchi, Y. Nakai, K. Nakamura, K. Ishizu, Y. Deguchi and H. Takaki, *Mol. Phys*. 1965 , **9**, 153-161.
9 a) E. De Boer, *Electronic Structure of Alkali Metal Adducts of Aromatic Hydrocarbons*, Adv. Organomet. Chem. Vol. 2, 1965, pp. 115-155; b) F. Gerson and W. Huber, *Electron Spin Resonance Spectroscopy of Organic Radicals*, 2003 Wiley-VCH Verlag GmbH & Co. KGaA, Weinheim, p. 113-114, 407.
10 J. J. Eisch, *J. Org. Chem.* **1963**, *28*, 707-710.
11 a) I. Blasco, H. Pérez and A. Guijarro, *J. Phys. Org. Chem.*, 2015, **28**, 388-395; b) C. Melero, H. Pérez, A. Guijarro and M. Yus, *Tetrahedron Lett.*, 2007, **48**, 4105-4109.
12 a) C. Melero, A. Guijarro and M. Yus, *Tetrahedron Lett.*, 2006, **47**, 6267-6271; b) C. Melero, A. Guijarro, V. Baumann, A. J. Pérez-Jimenez and M. Yus, *Eur. J. Org. Chem.* 2007, 5514-5526.
13 M. de la Viuda, M. Yus and A. Guijarro, *J. Phys. Chem. B*, 2011, **115**, 14610-14616.
14 $E°_2$ (BPh^{-2}/BPh^{-1}) = −3.18 V versus Ag/AgCl in Me_2NH (for comparison with Li, $E°$ (Ag/AgCl) = +0.22 V vs. NHE); only naphthalene has a more negative, yet to be measured $E°_2$: K. Meerholz and J. Heinze, *J. Am. Chem. Soc.* 1989, **111**, 2325-2326.
15 Lithium has the most negative reduction potential among alkali metals, with a formal reduction potential E^f_0 (Li/Li^+) = −3.48 V vs. $Fc/Fc^+PF_6^-$ in THF (for comparison with biphenyl, $Eº$ ($Fc/Fc^+PF_6^-$) = +0.40 V vs. NHE): C. A. Paddon, S. E. Ward

View Article Online
DOI: 10.1039/C7NJ04726F

Jones, F. L. Bhatti, T. J. Donohoe and R. G. J. Compton, *Phys. Org. Chem.* 2007, **20**, 677-684.
16 A. I. Shatenshtein and E. S. Petrov, *Russ. Chem. Rev.* 1967, **36**, 100-110.
17 K. H. J. Buschow, J. Dieleman and G. J. Hoijtink, *J. Chem. Phys.* 1965, **42**, 1993-1999.
18 R. K. Khanna, Y. M. Jiang, B. Srinivas, C. B. Smithhart and D. L. Wertz, *Chem. Mater.* 1993, **5**, 1792-1798.
19 M. Castillo, A. J. Metta-Magaña and S. Fortier, *New J. Chem*., 2016, **40**, 1923-1926.
20 a) P. Jørgensen and J. C. Poulsen, *J. Phys. Chem.* 1974, **78**, 1420-1422; b) P. Chang, R. V. Slates and M. Szwarc, *J. Phys. Chem.* 1966, **70**, 3180-3190; c) C. Takahashi and S. Maeda, *Chem. Phys. Lett.* 1974, **24**, 584-588; d) C. Lapouge, G. Buntinx and O. Poizat, *J. Mol. Struct. (Theochem)* 2003, **651-653**, 747-757; e) A. M. Funston, S. V. Lymar, B. Saunders-Price, G. Czapski and J. R. Miller, *J. Phys. Chem. B,* 2007, **111**, 6895-6902; f) S. Arai, A. Kira and M. Imamura, *J. Phys. Chem.* 1971, **54**, 5073-5081; g) J. Choi, D. W. Cho, S. Tojo, M. Fujitsuka and T. Majima, *J. Phys. Chem. A*, 2015, **119**, 851-856; h) A. Saeki, T. Kozawa, Y. Ohnishi and S. Tagawa, *J. Phys. Chem. A* 2007, **111**, 1229-1235.
21 P. Balk, G. J. Hoijtink and J. W. H. Schreurs, *Rec. Trav. Chim. Pays-Bas* 1957, **76**, 813-823.
22 A. Rembaum, A. Eisenberg, R. Haack and R. F. Landel, *J. Am. Chem. Soc.* 1967, **89**, 1062-1066.
23 G. Levin, B. E. Holloway and M. Szwarc, *J. Am. Chem. Soc.* 1976, **98**, 5706-5709.
24 S. V. Bondarchuk and B. F. Minaev, *J. Phys. Chem. A*, 2014, **118**, 8872-8882.
25 S. V. Bondarchuk and B. F. Minaev, *RSC Adv*., 2015, **5**, 11558-11569.
26 S. V. Bondarchuk and B. F. Minaev, *Phys. Chem. Chem. Phys*., 2017, **19**, 6698-6706.
27 S. V. Bondarchuk and B. F. Minaev, *J. Phys. Org. Chem*., 2014, **27**, 640-651.
28 S. V. Bondarchuk, B. F. Minaev and A. Yu. Fesak, *Int. J. Quantum Chem*., 2013, **113**, 2580-2588.
29 A) P. Balk, S. de Bruin and G. J. Hoijtink, *Rec. Trav. Chim.* 1957, **76**, 860-868; B) P. Balk, S. de Bruin and G. J. Hoijtink, *Rec. Trav. Chim.* 1957, **76**, 907-918.
30 M. Rubio, M. Merchán, E. Ortí and B. Roos, *J. Phys. Chem.* 1995, **99**, 14980-14987.
31 K. S. Tan, A. C. Grimsdale and R. Yazami, *J. Phys. Chem. B*, 2012, **116**, 9056-9060.
32 N. Liu, H. Li, J. Jiang, X. Huang and L. Chen, *J. Phys. Chem. B*, 2006, **110**, 10341-10347.
33 J. P. Devlin, J. S. McKennis, C. Thornton and J. C. Moore, *J. Phys. Chem.* 1982, **86**, 2613-2616.
34 I.V. Aleksandrov, Ya. S. Bobovich, V. G. Maslov and A. N. Sidorov, *Opt. Spectrosc.* 1975, **38**, 387-389.
35 G. I. Hoytink, *Chem. Phys. Lett.* 1975, **30**, 175-180.
36 W. Kohn and L. J. Sham, *Phys. Rev. A*, 1965, **140**, A1133-A1138.
37 M. J. Frisch, G. W. Trucks, H. B. Schlegel, G. E. Scuseria, M. A. Robb, J. R. Cheeseman, G. Scalmani, V. Barone, B. Mennucci and G. A. Petersson, *et al. Gaussian 09, Revision A.02*, Gaussian, Inc., Wallingford, CT, 2009.
38 A. D. Becke, *J. Chem. Phys*., 1993, **98**, 5648-5652.
39 C. Lee, W. Yang and R. G. Parr, *Phys. Rev. B*, 1988, **37**, 785-789.
40 R. Krishnan, J. S. Binkley, R. Seeger and J. A. Pople, *J. Chem. Phys*., 1980, **72**, 650-654.
41 S. Miertuš, E. Scrocco and J. Tomasi, *Chem. Phys*. 1981, **55**, 117-129.
42 R. E. Stratmann, G. E. Scuseria and M. J. Frisch, *J. Chem. Phys*. 1998, **109**, 8218-8224.
43 J.-D. Chai and M. Head-Gordon, *Phys. Chem. Chem. Phys*., 2008, **10**, 6615-6620.
44 O. A. Vydrov, G. E. Scuseria and J. P. Perdew, *J. Chem. Phys*., 2007, **126**, 154109.
45 T. Yanai, D. P. Tew and N. C. Handy, *Chem. Phys. Lett*., 2004, **393**, 51-57.
46 J. Heyd, G. E. Scuseria and M. Ernzerhof, *J. Chem. Phys*., 2006, **124**, 219906.
47 Y. Zhao and D. G. Truhlar, *Theor. Chem. Acc*., 2008, **120**, 215-241.
48 C. Adamo and V. Barone, *J. Chem. Phys*., 1998, **108**, 664-675.
49 Y. Zhao and D. G. Truhlar, *J. Chem. Phys*., 2006, **125**, 194101.
50 S. I. Gorelsky, SWizard program; University of Ottawa: Ottawa, Canada, 2013; http://www.sg-chem.net/.
51 R. F. W. Bader, *Atoms in molecules, a quantum theory*, Clarendon Press, Oxford, 1990.
52 T. A. Keith, *AIMAll, Version 10.07.25*, TK Gristmill Software, Overland Park, KS, 2010; http://www.aim.tkgristmill.com.
53 T. Lu and F. Chen, *J. Comp. Chem*., 2012, **33**, 580-592.
54 T. Lu and F. Chen, *J. Phys. Chem. A*, 2013, **117**, 3100-3108.
55 E. Espinosa, E. Molins and C. Lecomte, *Chem. Phys. Lett*. 1998, **285**, 170-.
56 F. de Proft, C. Van Alsenoy, A. Peeters, W. Langenaeker and P. Geerlings, *J. Comput. Chem*. 2002, **23**, 1198-1209.
57 J. P. Perdew, K. Burke and M. Ernzerhof. *Phys. Rev. Lett*., 1996, **77**, 3865-.
58 B. Delley, *J. Phys. Chem. A*, 2006, **110**, 13632-13639.
59 B. Delley, *J. Chem. Phys*. 1990, **92**, 508-517.
60 Materials Studio 7.0, Accelrys, Inc.: San Diego, CA, 2013.
61 A. Klamt, G. Schüürmann, *J. Chem. Soc., Perkin Trans. 2* 1993, 799-805.

View Article Online
DOI: 10.1039/C7NJ04726F

Table of contents entry

Short abstract:

A spontaneous disproportionation of lithium biphenyl radical anion —single component in crystalline state— into lithium biphenyl dianion plus neutral biphenyl —dominant species in solution—, according to 2LiBiph ⇄ Li_2Biph + Biph, has been evidenced experimentally by UV-vis spectroscopy and backed up theoretically by TDDFT methods.